

RESEARCH ARTICLE

10.1029/2018JD028776

Key Points:

- Small-magnitude eruptions caused a global-mean ERF of -0.08 W/m^2 during 2005–2015 relative to the volcanically quiescent 1999–2002 period
- In our model rapid adjustments act to reduce the total volcanic forcing per unit SAOD change by 13–21% for large-magnitude eruptions
- On average, frequent small-magnitude eruptions increase the nonvolcanic background SAOD by 0.004, equating to a volcanic ERF of -0.10 W/m^2

Supporting Information:

- Supporting Information S1

Correspondence to:

A. Schmidt,
anja.schmidt@ch.cam.ac.uk

Citation:

Schmidt, A., Mills, M. J., Ghan, S., Gregory, J. M., Allan, R. P., Andrews, T., et al. (2018). Volcanic radiative forcing from 1979 to 2015. *Journal of Geophysical Research: Atmospheres*, 123, 12,491–12,508. <https://doi.org/10.1029/2018JD028776>

Received 5 APR 2018

Accepted 11 OCT 2018

Accepted article online 24 OCT 2018

Published online 19 NOV 2018

Volcanic Radiative Forcing From 1979 to 2015

Anja Schmidt^{1,2} , Michael J. Mills³ , Steven Ghan⁴ , Jonathan M. Gregory^{5,6} , Richard P. Allan^{6,7} , Timothy Andrews⁸ , Charles G. Bardeen³ , Andrew Conley³ , Piers M. Forster⁹ , Andrew Gettelman³ , Robert W. Portmann¹⁰ , Susan Solomon¹¹ , and Owen B. Toon¹² 

¹Department of Chemistry, University of Cambridge, Cambridge, UK, ²Department of Geography, University of Cambridge, Cambridge, UK, ³Atmospheric Chemistry Observations and Modeling Laboratory, National Center for Atmospheric Research, Boulder, CO, USA, ⁴Atmospheric Sciences and Global Change Division, Pacific Northwest National Laboratory, Richland, WA, USA, ⁵NCAS-Climate, University of Reading, Reading, UK, ⁶Department of Meteorology, University of Reading, Reading, UK, ⁷National Centre for Earth Observation, Reading, UK, ⁸Met Office, Exeter, UK, ⁹School of Earth and Environment, University of Leeds, Leeds, UK, ¹⁰Chemical Sciences Division, NOAA Earth Systems Research Laboratory, Boulder, CO, USA, ¹¹Department of Earth, Atmospheric, and Planetary Sciences, Massachusetts Institute of Technology, Cambridge, MA, USA, ¹²Department of Atmospheric and Oceanic Sciences, Laboratory for Atmospheric and Space Physics, University of Colorado, Boulder, CO, USA

Abstract

Using volcanic sulfur dioxide emissions in an aerosol-climate model, we derive a time series of global-mean volcanic effective radiative forcing (ERF) from 1979 to 2015. For 2005–2015, we calculate a global multiannual mean volcanic ERF of -0.08 W/m^2 relative to the volcanically quiescent 1999–2002 period, due to a high frequency of small-to-moderate-magnitude explosive eruptions after 2004. For eruptions of large magnitude such as 1991 Mt. Pinatubo, our model-simulated volcanic ERF, which accounts for rapid adjustments including aerosol perturbations of clouds, is less negative than that reported in the Intergovernmental Panel on Climate Change (IPCC) Fifth Assessment Report (AR5) that only accounted for stratospheric temperature adjustments. We find that, when rapid adjustments are considered, the relation between volcanic forcing and volcanic stratospheric optical depth (SAOD) is 13–21% weaker than reported in IPCC AR5 for large-magnitude eruptions. Further, our analysis of the recurrence frequency of eruptions reveals that sulfur-rich small-to-moderate-magnitude eruptions with column heights $\geq 10 \text{ km}$ occur frequently, with periods of volcanic quiescence being statistically rare. Small-to-moderate-magnitude eruptions should therefore be included in climate model simulations, given the $>50\%$ chance of one or two eruptions to occur in any given year. Not all of these eruptions affect the stratospheric aerosol budget, but those that do increase the nonvolcanic background SAOD by ~ 0.004 on average, contributing $\sim 50\%$ to the total SAOD in the absence of large-magnitude eruptions. This equates to a volcanic ERF of about -0.10 W/m^2 , which is about two thirds of the ERF from ozone changes induced by ozone-depleting substances.

Plain Language Summary

We calculate the climatic effects of explosive volcanic eruptions between 1979 and 2015 using a more complex climate model simulation than has been used previously. This includes many of the chemical and physical processes that lead to the formation of volcanic aerosol. Volcanic aerosols are tiny airborne particles that are important for Earth's climate because they reflect sunlight and trap thermal infrared radiative energy. In line with previous studies, we find that the most powerful eruptions between 1979 and 2015 had a substantial cooling effect. However, we calculate that their effect on climate is about 20% weaker than previous estimates used by the Intergovernmental Panel on Climate Change (IPCC). In our model simulation this is mainly a result of the volcanic aerosol particles affecting ice clouds, making these clouds less transparent. We also find that it is very rare to have a period with relatively few notable explosive eruptions as was the case during 1996–2002. Furthermore, eruptions of small-to-moderate size occur frequently and decrease the transparency of the stratosphere by as much as all nonvolcanic sources of aerosol particles combined. These small-sized volcanic eruptions therefore cause a small but noticeable surface cooling and so should be included in climate model simulations, which is rarely done.

1. Introduction

Radiative forcing from human activity is primarily responsible for the warming of climate since the 1950s, yet increases in global surface temperature have not progressed smoothly (Fyfe, Gillett, et al., 2013; Morice et al.,

2012). Changes in the decadal rate of global warming have been attributed to several factors including internal climate variability (Marotzke & Forster, 2015) thought to be driven mainly by variability in the Pacific Decadal Oscillation (Trenberth & Fasullo, 2013), biases and variability arising from the treatment of the surface temperature observations themselves (Cowtan & Way, 2014; Karl et al., 2015), and temporal changes in natural and anthropogenic forcings such as tropospheric anthropogenic aerosol, solar irradiance, and volcanic eruptions (Haywood et al., 2014; Monerie et al., 2017; Santer et al., 2014; Schmidt et al., 2014; Solomon et al., 2011).

Quantifying human-caused climate change and the effectiveness of mitigation strategies demands the accurate attribution of present and future changes of Earth's energy budget and surface temperature not only to anthropogenic but also to natural climate forcing agents such as volcanic eruptions. Previous work found a statistically significant correlation between the occurrence of a series of small-to-moderate-magnitude explosive volcanic eruptions since the year 2000 and observed temperature changes in the lower troposphere (Santer et al., 2014). It has also been shown that climate models that neglect forcing from volcanic eruptions since the year 2000 tend to project a faster rate of global warming for the first 15 years of the 21st century than those models including this volcanic forcing (Fyfe, Gillett, et al., 2013; Santer et al., 2014; Schmidt et al., 2014; Solomon et al., 2011). The volcanic forcing time series used in those studies were based on satellite-derived estimates of volcanic stratospheric aerosol optical depth (SAOD) above 380 K in potential temperature (Vernier et al., 2011), that is about 17 km above sea level in the tropics and about 14 km at midlatitudes.

Historically, the volcanic SAOD data sets used to force climate models were restricted to altitudes above 380 K in potential temperature because (1) this is where initially most of the volcanic aerosol following large-magnitude explosive eruptions resides and (2) retrieving aerosol properties is challenging when dense volcanic aerosol plumes and/or liquid water and ice clouds are present near or below 380 K (Andersson et al., 2015; Fromm et al., 2014). However, analysis of lidar, Aerosol Robotic Network, and balloon-borne data suggests that depending on location, season, and volcanic activity, up to 70% of the volcanic SAOD between 2004 and 2015 resided in the lowermost stratosphere (Ridley et al., 2014; defined as the region between the tropopause and the 380 K potential temperature level). Comparisons of spaceborne measurements and aircraft measurements also suggest that on average 30% of the global SAOD between 2008 and 2011 resided in the lowermost stratosphere (Andersson et al., 2015). Aerosol-climate model simulations of volcanic aerosol properties from 1990 to 2014 similarly suggest that following the 2008 Kasatochi eruption, up to 54% of the global SAOD resided in the lowermost stratosphere (Mills et al., 2016), in good agreement with lidar, spaceborne, and aircraft measurements (Andersson et al., 2015; Ridley et al., 2014). Therefore, to accurately represent the magnitude of volcanic forcing of climate and its potential contribution to global warming rates, climate model simulations should account for lowermost stratosphere volcanic aerosol as demonstrated by several studies (Schmidt et al., 2014; Solomon et al., 2011) using up-to-date satellite-based volcanic SAOD data sets (Thomason et al., 2018).

Instead of prescribing a satellite-based SAOD data set, we derive a time series of global-mean volcanic effective radiative forcing (ERF) for the period 1979 to 2015, accounting for volcanic aerosol in the lowermost stratosphere and rapid adjustments (including atmospheric temperature and clouds among others), by using a detailed volcanic sulfur dioxide (SO₂) emission inventory in a climate model (Community Earth System Model version 1 [CESM1]) with comprehensive sulfur chemistry and a prognostic stratospheric aerosol scheme (Whole Atmosphere Community Climate Model with a modal aerosol module [WACCM-MAM]). As far as we are aware there is only one other study to date by Ge et al. (2016), which used an emission-based approach to derive a volcanic forcing time series for the period 2005 to 2012 in an aerosol-climate model. Crucially, in contrast to our study, Ge et al. (2016) do not account for the contributions of aerosol-cloud interactions and longwave (LW) forcings to the total volcanic forcing. In our study, we decompose the total volcanic ERF into contributions from aerosol-radiation interactions and aerosol-cloud interactions. We also present a statistical analysis of the recurrence frequencies of explosive eruptions of different magnitudes and discuss their effects on the stratospheric aerosol budget and radiative forcing of global climate.

2. Methods

2.1. CESM1(WACCM) Model Setup

Simulations were run over the period January 1979 to December 2015 using CESM1 with WACCM-MAM at a resolution of 1.9° latitude × 2.5° longitude. WACCM includes a prognostic modal aerosol module and a

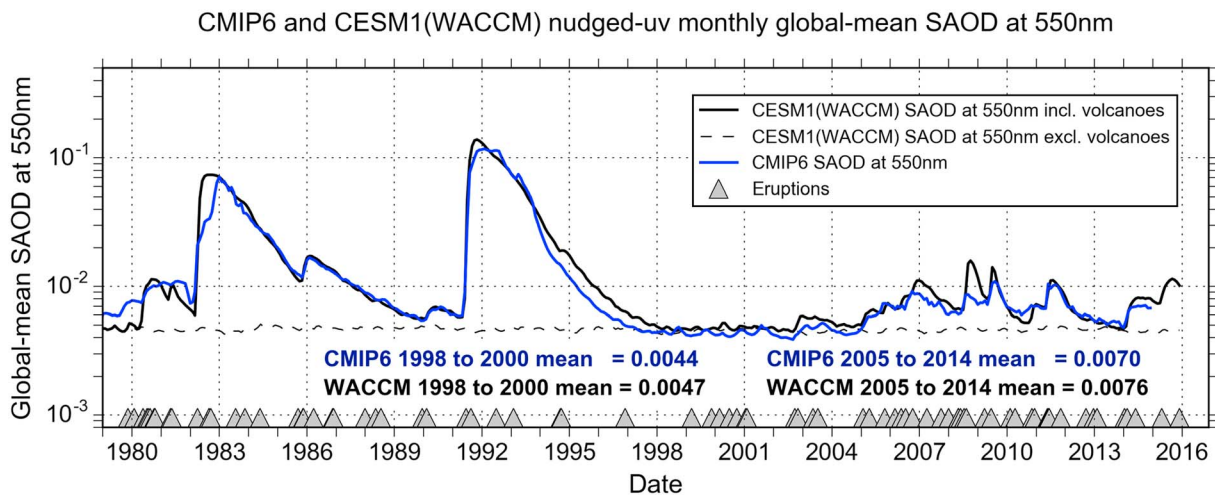


Figure 1. Comparison of Coupled Model Inter-comparison Project version 6 (CMIP6; blue line) and model-simulated (solid black line = including volcanic sulfur dioxide emissions, dashed black line = omitting volcanic sulfur dioxide emissions) monthly global-mean stratospheric aerosol optical depth (SAOD) at 550 nm.

detailed sulfur chemistry scheme (Mills et al., 2016). As described in Mills et al. (2016) sulfur emitted from anthropogenic and natural sources such as dimethyl sulfide (DMS) and carbonyl sulfide (OCS) is accounted for in the simulations. To diagnose the volcanic ERF, we run one simulation with and one without volcanic sulfur dioxide (SO_2) emissions. The volcanic SO_2 emission inventory (Neely & Schmidt, 2016) has been used and described previously (Mills et al., 2016; Solomon et al., 2016). Briefly, the inventory contains volcanic eruptions that emitted SO_2 either directly into the stratosphere or the upper troposphere. The emission inventory containing information on the mass of SO_2 emitted and volcanic plume heights for eruptions that had a measurable SO_2 signal was compiled based on a variety of published and/or freely available measurements from satellites including Total Ozone Mapping Spectrometer (TOMS), Ozone Monitoring Instrument (OMI), Ozone Mapping Profile Suite (OMPS), Infrared Atmospheric Sounding Interferometer (IASI), Global Ozone Monitoring Experiment (GOME/2), Atmospheric Infrared Sounder (AIRS), Microwave Limb Sounder (MLS), Michelson Interferometer for Passive Atmospheric Sounding (MIPAS), and ground-based remote sensing or petrological methods. The plume heights were compiled based on published estimates of the eruption source parameters and reports from the Smithsonian Global Volcanism Program (<http://volcano.si.edu/>), National Aeronautics and Space Administration (NASA)'s Global Sulfur Dioxide Monitoring website (<http://so2.gsfc.nasa.gov/>), and the Support to Aviation Control Service (<http://sacs.aeronomie.be/>). Several other volcanic SO_2 emission inventories exist (Bingen et al., 2017; Brühl et al., 2015; Carn et al., 2016; Diehl et al., 2012), and a detailed comparison of the differences and similarities can be found in Timmreck et al. (2018).

Model simulations were run specifying time-varying historical sea surface (but not land surface) temperatures and sea ice (Hurrell et al., 2008). Zonal and meridional winds and surface pressures from the lowermost atmospheric layer to 50 km were relaxed with a 50-hr timescale toward meteorological reanalysis fields from the NASA Global Modeling and Assimilation Office Modern-Era Retrospective Analysis for Research and Applications (MERRA; Rienecker et al., 2011). This setup, referred to as *nudged-uv* from here on (where u and v denote the eastward and northward components of wind), improves consistency between the simulated and observed meteorological conditions, but means our ERF will not include the radiative impact of any circulation changes induced by volcanic aerosol particles (see section 2.2).

In Mills et al. (2016), we compared model-simulated volcanic aerosol properties such as SAOD for both large-magnitude eruptions and smaller magnitude volcanic eruptions to a range of in situ and remote-sensing observations. Figure 1 shows that the model-simulated SAOD at 550 nm compares very well to the Coupled Model Inter-comparison Project phase 6 (CMIP6) SAOD (downloaded from ftp://iacftp.ethz.ch/pub_read/luo/CMIP6/) during a volcanically quiescent period (1998–2000) and a period of frequent volcanic activity (2005–2014). The CMIP6 SAOD data set from 1979 onward is further described in Thomason et al. (2018).

2.2. Diagnosing Volcanic Effective Radiative Forcings

Applying nudged u and v components of the wind in our model simulations, although still an imperfect approach, has the advantage of ensuring that the volcanic ERF we diagnose is minimally influenced by atmospheric adjustments due to circulation changes. Such adjustments affect other methods of diagnosing ERF, such as those based on either prescribed sea surface temperature or regression approaches (Forster et al., 2016). Several studies showed that ERFs including the radiative effects from aerosol-cloud interactions can be diagnosed from nudged- uv simulations with similar accuracy to that obtainable from methods where only sea surface temperatures and sea ice are prescribed (Forster et al., 2016; Kooperman et al., 2012; Zhang et al., 2014). In our case nudging the wind components allows us to isolate relatively small forcings because natural variability and climate feedback are largely the same in simulations with and without volcanic emissions, while other factors such as clouds and stratospheric temperatures are allowed to adjust under the presence of volcanic sulfate aerosol particles. However, as a consequence, certain rapid adjustments, such as cloud cover changes due to changes in dynamics, are unaccounted for in our setup, whereas adjustments via changes in both liquid water and ice cloud microphysical properties (i.e., particle number concentrations and particle size) are accounted for. Therefore, the nudged- uv volcanic ERF (hereafter referred to as *volcanic ERF*) diagnosed from our simulations can be thought of as a partially adjusted ERF, which does not correspond exactly to the Intergovernmental Panel on Climate Change (IPCC) definitions of either ERF or Instantaneous Radiative Forcing (IRF) (Forster et al., 2016). To characterize some of the limitations of our approach, we compare the results to a set of free-running simulations with specified time-varying sea surface temperatures and sea ice.

We decompose the volcanic ERF (ΔF in equation (1)) into its components by applying a previously developed method (Ghan, 2013) and extending it to the LW forcing.

$$\Delta F = \Delta(F - F_{\text{clean}}) + \Delta(F_{\text{clean}} - F_{\text{clean,clear}}) + \Delta F_{\text{clean,clear}} \quad (1)$$

where F is the net (positive downward) radiative (shortwave [SW] or LW) flux at the top of the atmosphere and Δ denotes the difference between simulations with and without volcanic SO_2 emissions. The decomposition is enabled by implementing extra calls to the radiation code to obtain F_{clean} and $F_{\text{clean,clear}}$ in both simulations (see below for further details). F_{clean} denotes a diagnostic calculation of the flux that ignores scattering and absorption by *all* aerosols (not just volcanic aerosol), but it includes aerosol-cloud interactions through microphysics. $F_{\text{clean,clear}}$ denotes a diagnostic calculation that ignores the radiative effects of clouds as well as aerosols. In the model, microphysical effects of sulfur on cloud droplet and cloud ice mass mixing ratios and number concentrations are represented in a two-moment cloud microphysics scheme (Morrison & Gettelman, 2008), which also includes process-based treatments of ice microphysics such as ice nucleation (Gettelman et al., 2010). The ice nucleation scheme used is the same as described in Mills et al. (2017) except for one update to the homogeneous freezing routine to enable coarse-mode sulfate aerosol particles to nucleate ice via homogeneous freezing. $F - F_{\text{clean}}$ therefore determines the impact of *all* aerosols on F through aerosol-radiation interactions, so the first term $\Delta(F - F_{\text{clean}})$ is an estimate of forcing from aerosol-radiation interactions (ERFari) due to volcanic emissions. The second term $\Delta(F_{\text{clean}} - F_{\text{clean,clear}})$, the difference in the *clean-sky* cloud radiative forcing, is an estimate of forcing from aerosol-cloud interactions (ERFaci) due to volcanic emissions. The third term $\Delta F_{\text{clean,clear}}$ accounts for changes in surface albedo in the SW and in the LW for changes such as surface temperature and water vapor profiles (i.e., changes not due directly to aerosol or cloud).

In more detail, the model diagnostics are as follows:

- S = net positive downward shortwave flux at top of atmosphere (TOA)
- S_{clear} = clear-sky net positive downward shortwave flux at TOA
- S_{clean} = net positive downward shortwave flux at TOA that ignores scattering and absorption by *all* aerosols (not just volcanic aerosol)
- $S_{\text{clean,clear}}$ = clear-sky net positive downward shortwave flux at TOA that ignores scattering and absorption by *all* aerosols (not just volcanic aerosol)
- L = net positive downward longwave flux at TOA

L_{clear} = clear-sky net positive downward longwave flux at TOA
 L_{clean} = net positive downward longwave flux at TOA that ignores scattering and absorption by *all* aerosols (not just volcanic aerosol)
 $L_{\text{clean,clear}}$ = clear-sky net positive downward longwave flux at TOA that ignores scattering and absorption by *all* aerosols (not just volcanic aerosol).

Each of these quantities is diagnosed in the simulations both with and without volcanic SO₂ emissions, denoted by ^V and ^N respectively.

SW forcing from aerosol-radiation interactions:

$$dSW_ERFari = \Delta (S - S_{\text{clean}}) = (S^V - S_{\text{clean}}^V) - (S^N - S_{\text{clean}}^N)$$

SW forcing from aerosol-cloud interactions:

$$dSW_ERFaci = \Delta (S_{\text{clean}} - S_{\text{clean,clear}}) = (S_{\text{clean}}^V - S_{\text{clean,clear}}^V) - (S_{\text{clean}}^N - S_{\text{clean,clear}}^N)$$

SW surface albedo forcing:

$$dSW_ERFa = \Delta (S_{\text{clean,clear}}) = S_{\text{clean,clear}}^V - S_{\text{clean,clear}}^N$$

LW forcing from aerosol-radiation interactions:

$$dLW_ERFari = \Delta (L - L_{\text{clean}}) = (L^V - L_{\text{clean}}^V) - (L^N - L_{\text{clean}}^N)$$

LW forcing from aerosol-cloud interactions:

$$dLW_ERFaci = \Delta (L_{\text{clean}} - L_{\text{clean,clear}}) = (L_{\text{clean}}^V - L_{\text{clean,clear}}^V) - (L_{\text{clean}}^N - L_{\text{clean,clear}}^N)$$

LW atmosphere adjustment and surface albedo forcing:

$$dLW_ERFa = \Delta (L_{\text{clean,clear}}) = L_{\text{clean,clear}}^V - L_{\text{clean,clear}}^N$$

Total forcing from aerosol-radiation interactions:

$$ERFari = dSW_ERFari + dLW_ERFari$$

Total forcing from aerosol-cloud interactions:

$$ERFaci = dSW_ERFaci + dLW_ERFaci$$

2.3. Energy Budget Model Calculations

To illustrate the effects of our volcanic ERF time series on Earth's energy budget and surface temperature changes, we used a globally averaged energy budget model (Forster & Gregory, 2006). The model's main output is change in surface temperature, which is taken to be the globally averaged temperature of a 100-m mixed layer of ocean. We applied annual globally averaged time series of volcanic ERF for different scenarios as detailed in Table 1, while other natural and anthropogenic forcings were kept the same for each volcanic forcing scenario and were taken from IPCC (Intergovernmental Panel on Climate Change, 2013) and from 2012 onward using future scenario data (Meinshausen et al., 2011; Representative Concentration Pathway 4.5). For each scenario the model evolves the energy imbalance and temperature changes through time. The changes in energy budget between 1979 and 2011 resulting from applying our volcanic ERF time series are calculated relative to the volcanic forcing used by IPCC (IPCC, 2013). In our setup, the surface temperature response is calculated assuming a constant diffusivity of 0.001 m²/s within the underlying 900-m-deep ocean, along with a Planck response and climate feedback response that emits energy to space

Table 1
Annual Global-Mean Volcanic Forcings (W/m^2) Applied in Energy Budget Model, and Total Forcing Reported in IPCC AR5

Year	This study	Schmidt et al. (2014)	IPCC AR5 volcanic forcing	IPCC AR5 total forcing	Sato et al. (1993, 2002 update)
1979	+0.03	–	–0.23	1.15	–0.24
1980	–0.16	–	–0.13	1.28	–0.12
1981	–0.28	–	–0.13	1.31	–0.13
1982	–1.21	–	–1.33	0.08	–1.37
1983	–1.24	–	–1.88	–0.43	–2.0
1984	–0.69	–	–0.75	0.65	–0.78
1985	–0.43	–	–0.33	1.11	–0.33
1986	–0.37	–	–0.35	1.11	–0.35
1987	–0.12	–	–0.25	1.26	–0.27
1988	–0.17	–	–0.2	1.43	–0.2
1989	–0.18	–	–0.15	1.57	–0.16
1990	–0.05	–0.14	–0.15	1.57	–0.15
1991	–1.25	–1.12	–1.35	0.40	–1.35
1992	–2.39	–2.09	–3.03	–1.24	–3.03
1993	–1.23	–0.87	–1.23	0.50	–1.23
1994	–0.63	–0.36	–0.50	1.22	–0.50
1995	–0.26	–0.19	–0.25	1.49	–0.24
1996	–0.09	–0.13	–0.18	1.58	–0.16
1997	–0.06	–0.11	–0.13	1.67	–0.13
1998	+0.01	–0.10	–0.08	1.80	–0.07
1999	–0.04	–0.10	–0.05	1.90	–0.05
2000	–0.10	–0.10	–0.05	1.95	–0.003
2001	+0.003	–0.10	–0.05	1.97	–0.003
2002	–0.02	–0.10	–0.05	1.0	–0.003
2003	–0.08	–0.12	–0.08	1.95	–0.003
2004	–0.04	–0.11	–0.05	1.99	–0.003
2005	–0.08	–0.14	–0.08	1.98	–0.003
2006	–0.13	–0.15	–0.10	1.99	–0.003
2007	–0.24	–0.17	–0.10	2.02	–0.003
2008	–0.03	–0.15	–0.10	2.05	–0.003
2009	–0.26	–0.14	–0.13	2.06	–0.003
2010	–0.09	–0.12	–0.10	2.16	–0.003
2011	–0.11	–0.15	–0.13	2.20	–0.003
2012	–0.10	–0.12	–	–	–0.003
2013	–0.03	–	–	–	–
2014	–0.12	–	–	–	–
2015	–0.17	–	–	–	–

Note. IPCC AR5 data available at http://www.climatechange2013.org/images/report/WG1AR5_AISSM_Datafiles.xlsx.

to help restore the energy imbalance. This emission to space is given as $Y\Delta T$, where ΔT is the mixed layer temperature change and Y is a climate feedback parameter directly connected to the equilibrium climate sensitivity (ECS), such that $ECS = F_2 \times CO_2 / Y$, where $F_2 \times CO_2$ is the forcing for a doubling of carbon dioxide ($+3.7 W/m^2$). To calculate the temperature changes, we set Y to $1.3 W \cdot m^{-2} \cdot K^{-1}$, which corresponds to an ECS of 2.85 K.

3. Results and Discussion

3.1. Volcanic Eruptions and Volcanic Effective Radiative Forcing 1979–2015

Figure 2 shows the occurrence of explosive volcanic eruptions and the volcanic ERF these eruptions exerted between the years 1979 and 2015. Here we define small-to-moderate-magnitude volcanic eruptions as those with a Volcanic Explosivity Index (VEI; Newhall & Self, 1982) of 3, 4, or 5 and emitting a mass of SO_2 of at least 0.01 Tg into altitudes of 10 km or above. Briefly, the period 1979 to 2015 is characterized by 18 such small-to-moderate-magnitude volcanic eruptions in the 1980s, which emitted a combined total of about 6.3 Tg of SO_2 , 6 such eruptions in the 1990s that emitted about 1.4 Tg of SO_2 , 22 in the 2000s that emitted about 5.3 Tg of SO_2 , and 10 in the 6 years between 2010 and the end of 2015 that emitted about 3.7 Tg of SO_2 . The 2000–2015 period was dominated by VEI 3 and VEI 4 eruptions, whereas the 1990s saw one VEI 5 eruption and the last VEI 6 eruption to date (1991 Mt. Pinatubo). Between July 2008 and May 2011, a notable series of seven VEI 3–4 eruptions occurred in the midlatitudes of the Northern Hemisphere, emitting a combined total of 4.4 Tg of SO_2 mainly into the lowermost stratosphere. There also was a series of three VEI 4–5 eruptions between May 2008 and April 2015 in the midlatitudes of the Southern Hemisphere, emitting a total of 0.66 Tg of SO_2 . Notably, these were the first VEI 4 and 5 eruptions since Cerro Hudson in 1991 in the Southern Hemisphere.

Averaged over the 2005–2015 period, which saw a high frequency of VEI 3, 4, and 5 volcanic eruptions in the midlatitudes of the Northern Hemisphere (Figure 2), the global-mean volcanic ERF in our model is about $-0.12 W/m^2$ (diagnosed as the difference between simulations with and without volcanic SO_2 emissions, ΔF in equation (1); see section 2.2). The volcanic ERF we calculate (Figure 2 and Table 1) is in very good agreement with previous work (Solomon et al., 2011), and IPCC's Fifth Assessment Report (AR5) estimate of $-0.11 W/m^2$ (-0.15 to $-0.08 W/m^2$) for the period 2008–2011 (Myhre et al., 2013). The 1999–2002 period was characterized by relative volcanic quiescence given that only seven eruptions occurred, emitting a combined total of 0.5 Tg of SO_2 (Figure 2b). Our global multiannual mean volcanic ERF of $-0.04 W/m^2$ for the period 1999 to 2002 is in good agreement with the IPCC AR5 estimate of $-0.06 W/m^2$ (-0.08 to $-0.04 W/m^2$) (Myhre et al., 2013) for the same period. The change in global-mean volcanic ERF of about $-0.08 W/m^2$ from $-0.04 W/m^2$ for 1999–2002 to $-0.12 W/m^2$ for 2005–2015 can be compared with the increase in time-mean carbon dioxide (CO_2) forcing of $+0.26 W/m^2$ between the same two periods (National Oceanic and Atmospheric Administration [NOAA], 2016a). Consequently, the change in global-mean volcanic ERF offsets $\sim 31\%$ of the change in global-mean CO_2 forcing according to our model simulations. It is therefore important to include post-2004 small-to-moderate-magnitude eruptions in Earth system model simulations to accurately simulate decadal timescale climate changes.

Figure 3 shows that for both the period following the 1991 Mt. Pinatubo eruption (1991–1994) and the 2000–2015 period the model-simulated net global-mean radiative flux anomalies are in reasonable agreement (R of 0.78 and 0.80, respectively) with satellite-derived fluxes using merged Earth Radiation Budget Satellite (ERBS)

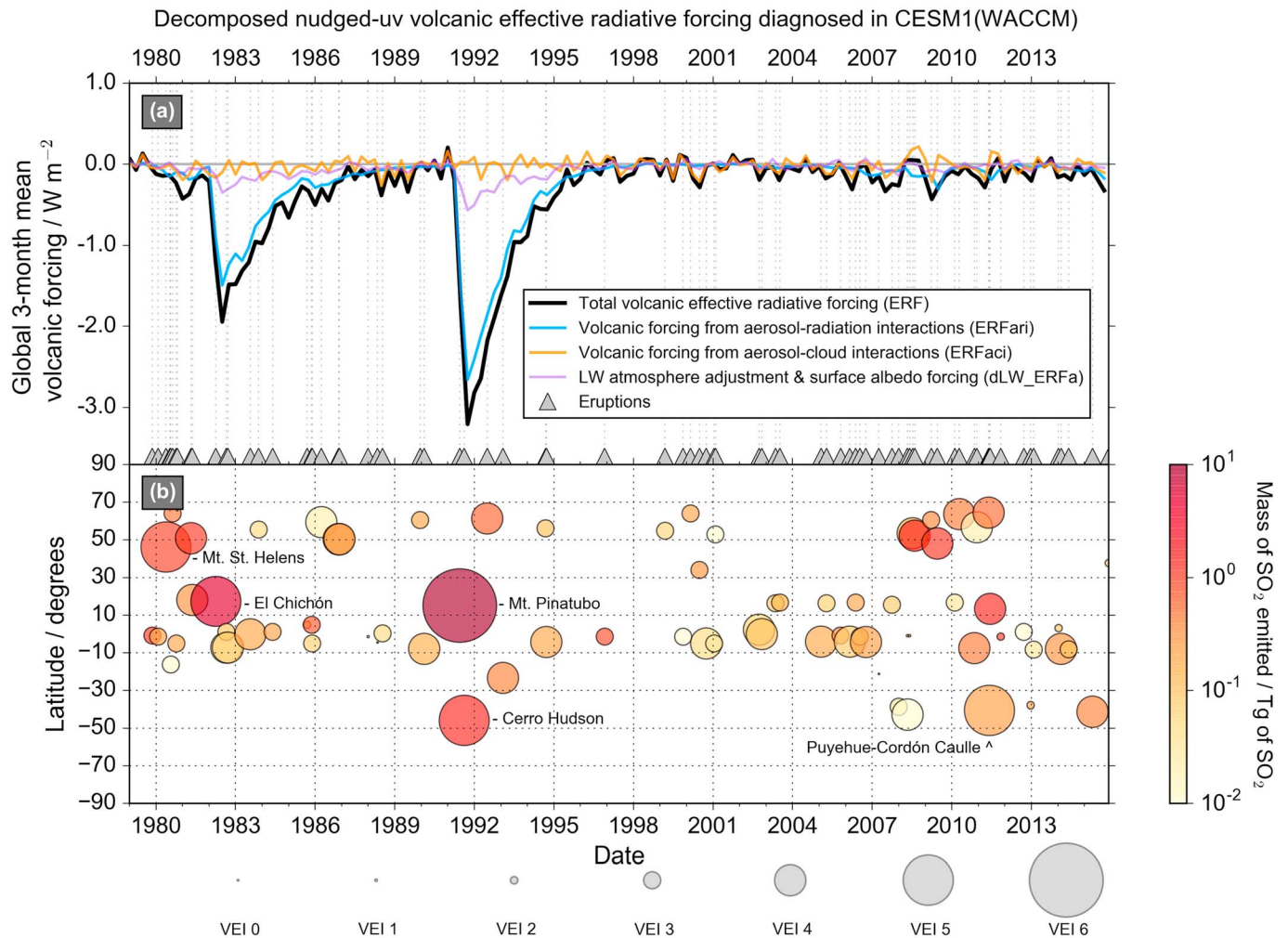


Figure 2. Time series of (a) global 3-month mean nudged-uv total volcanic effective radiative forcing (ERF, in W/m^2 , black line) diagnosed in CESM1-WACCM as the difference between simulations with and without volcanic emissions. The volcanic ERF is further decomposed into the forcings from aerosol-radiation interactions (ERFari, blue line) and aerosol-cloud interactions (ERFaci, orange line), and a longwave atmosphere adjustment and surface albedo term (dLW_ERFa, purple line; see section 2). (b) A time series of volcanic sulfur dioxide (SO_2) emissions (in Tg of SO_2 , shown by the color) used in our simulations as a function of latitude, with the eruption size (indicated by seven distinct sizes of grey circles) using the Volcanic Explosivity Index (VEI; Newhall & Self, 1982).

data and measurements from the Clouds and the Earth's Radiant Energy System (CERES EBAF v4.0; Loeb et al., 2017). In line with previous work (e.g., Forster & Taylor, 2006; Hansen et al., 2005), we find that volcanic ERF from aerosol-radiation interactions (ERFari; blue line Figure 2a) dominates the total volcanic ERF (black line Figure 2) following large-magnitude explosive eruptions such as 1991 Mt. Pinatubo. For 1991 Mt. Pinatubo, we calculate a peak global monthly mean net radiative flux anomaly of $-3.2 W/m^2$ in September 1991 (Figure 2), in good agreement with the peak radiative flux anomaly derived from $60^{\circ}S$ to $60^{\circ}N$ ERBS satellite broadband nonscanner measurements during the Earth Radiation Budget Experiment (ERBE; Minnis et al., 1993), which were merged with additional data to provide continuous monthly global coverage (Allan et al., 2014).

To date, few studies have investigated the role of rapid adjustments including the forcing from aerosol-cloud interactions (ERFaci) in modulating the total forcing from large-magnitude volcanic eruptions (Gregory et al., 2016; Hansen et al., 2005; Larson & Portmann, 2016), and as far as we are aware no study focused on deriving a volcanic ERF time series that accounts for both large-magnitude and small-to-moderate-magnitude eruptions. Figures 2a and 4 highlight that in our simulations, ERFaci (orange line in Figure 2a) is small (range of

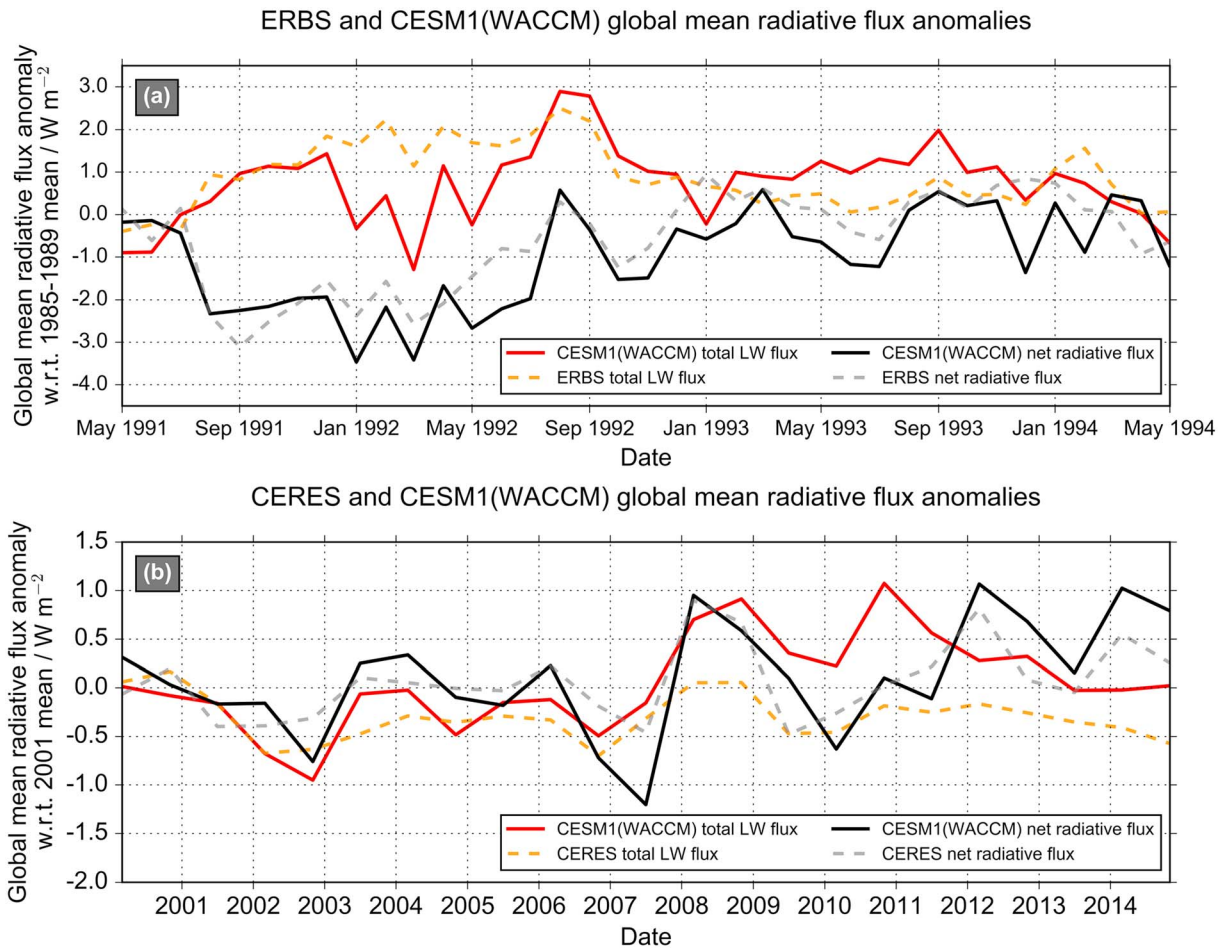


Figure 3. Time series of model-simulated net (solid black lines) and total longwave (LW, solid red line) downward radiative flux anomalies compared to deseasonalized satellite broadband anomalies (dashed lines) from (a) the Earth Radiation Budget Satellite (ERBS; Minnis et al., 1993) merged with additional data to provide a global data set (Allan et al., 2014) (anomalies calculated with respect to 1985–1989 mean) and (b) the Clouds and the Earth’s Radiant Energy System (CERES EBAF v4.0; Loeb et al., 2017) (anomalies calculated with respect to 2001 mean).

–0.27 and + 0.22 W/m^2) compared to ERFari (minimum of –2.67 W/m^2) and of similar magnitude no matter what the magnitude of an eruption. For the 2005 to 2015 period, when there were no VEI 6 eruptions, the model-simulated total LW forcing is dominated by the LW forcing from aerosol-cloud interactions (dLW_ERFaci). This is in contrast to the 1991–1994 Pinatubo period, when the LW forcing from aerosol-radiation interactions dominated (Figure 4). For both the El Chichón period (1982–1985) and the Pinatubo period (1991–1994), ERFari dominated because a large amount of sulfate was carried high into the stratosphere (Figure S1) by the rising branch of the Brewer-Dobson circulation, which was accelerated by heating in the volcanic cloud, causing strong reflection of SW radiation that exceeds absorption of outgoing LW radiation. For eruptions after 2004, the total SW radiative flux anomalies are smaller than during the Pinatubo period and of comparable magnitude to the total LW forcing (Figure 4). This is mainly a result of lower SO_2 masses emitted into lower altitudes (upper troposphere/lower stratosphere) after the year 2004, which results in reduced sulfate aerosol mass mixing ratios and shorter aerosol particle lifetimes in the stratosphere compared to the Pinatubo period (Figure S1). This in turn increases the relative importance of aerosol-cloud interactions in both the LW and SW for small-to-moderate-magnitude eruptions compared to larger-magnitude eruptions like 1991 Mt. Pinatubo.

While the model-simulated net and LW downward radiative flux anomalies are in reasonable agreement with satellite-based estimates for the Mt. Pinatubo period, Figure 3 clearly shows that for the period between 2008 and 2015, the model overestimates both the global-mean SW and LW flux anomalies; the latter by up to

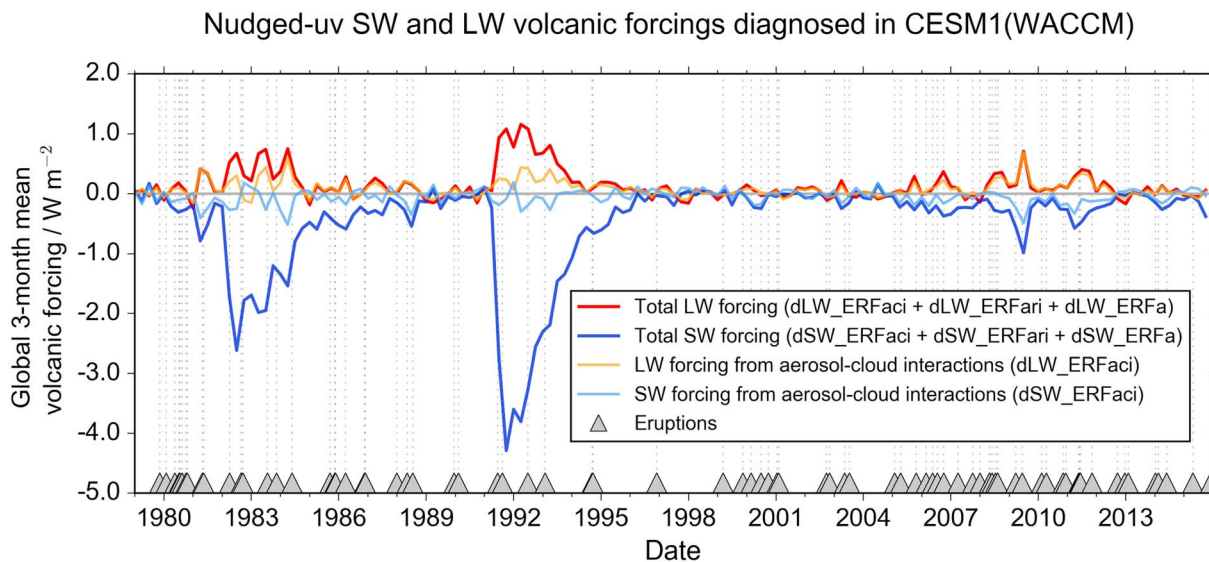


Figure 4. Time series of monthly global 3-month mean nudged-uv total shortwave (SW) volcanic forcing (in units of W/m^2 , blue line) and total longwave (LW) volcanic forcing (red line) diagnosed in CESM1-WACCM from simulations with and without volcanic sulfur dioxide emissions. The light blue line shows the SW volcanic forcing from aerosol-cloud interactions (dSW_ERFaci), and the yellow line shows the LW volcanic forcing from aerosol-cloud interactions (dLW_ERFaci). The grey triangles refer to eruptions represented in the volcanic sulfur dioxide emission inventory used for the simulations.

1.26 W/m^2 (0.67 W/m^2 on average) when compared to CERES. For CERES, monthly random errors in mean radiative fluxes are estimated to be $\sim 0.2 \text{ W/m}^2$ (Loeb et al., 2012). In our model, the LW flux anomalies in 2008–2015 are dominated by a large effect from aerosol-cloud interactions on LW radiation (dLW_ERFaci; yellow line in Figure 4), which results from an increase in the number concentration of ice crystals and a decrease in their size (Figure 5) due to the additional sulfur in the upper troposphere/lower stratosphere (Figure S1). Gettelman et al. (2012) and Ghan et al. (2012) found similar-magnitude effects of anthropogenic sulfur emissions on LW radiative forcing via aerosol modification of cirrus clouds in the Community Atmosphere Model version 5. At present there are no conclusive observations (Friberg et al., 2015; Luo et al., 2002; Sassen, 1992) to confirm or rule out the role of volcanic sulfuric acid particles in altering the properties of ice clouds. Moreover, the results from model studies that investigate the effects of either sulfate geoengineering or volcanic eruptions on the thermodynamic and microphysical properties of cirrus clouds remain equivocal, with the resulting changes in cloudiness, ice crystal number, and mass concentrations strongly depending on the freezing parameterization, the aerosol scheme used, and the aerosol size-number distribution produced by an eruption (e.g., Cirisan et al., 2013; Jensen & Toon, 1992; Kuebbeler et al., 2012; Lohmann et al., 2003; Visioni et al., 2018). For instance, Jensen and Toon (1992) found an increase in particle number concentrations as a result of large sulfate aerosol particles sedimenting out of the stratosphere and nucleating homogeneously, a reduction of number when heterogeneous nuclei came from the volcanic cloud, and little change when particles were added that were identical to those already present. Several factors including vertical air speeds (cooling rate), the ability of the added particles to impact supersaturation with respect to ice, and the size of the additional particles determine the rate and limits of homogeneous nucleation. Thus, particle number concentration could theoretically either increase or decrease, and satellite data and in situ measurements of the occurrence frequency and microphysical properties of cirrus clouds before and after future eruptions would be highly desirable to better understand the significance of this type of aerosol-cloud interaction.

3.2. Regression of Volcanic Effective Radiative Forcing Against SAOD

The relationship between volcanic ERF and SAOD is a key metric used to quantify the volcanic forcing of climate and to subsequently contrast volcanic sulfate forcing efficacy to other climate forcing agents (Hansen et al., 2005). In IPCC AR5 (Myhre et al., 2013), a relation between volcanic forcing (ΔF in W/m^2) and volcanic SAOD changes (τ) of $\Delta F \sim -25 \text{ W/m}^2$ per unit volcanic SAOD change is used. The

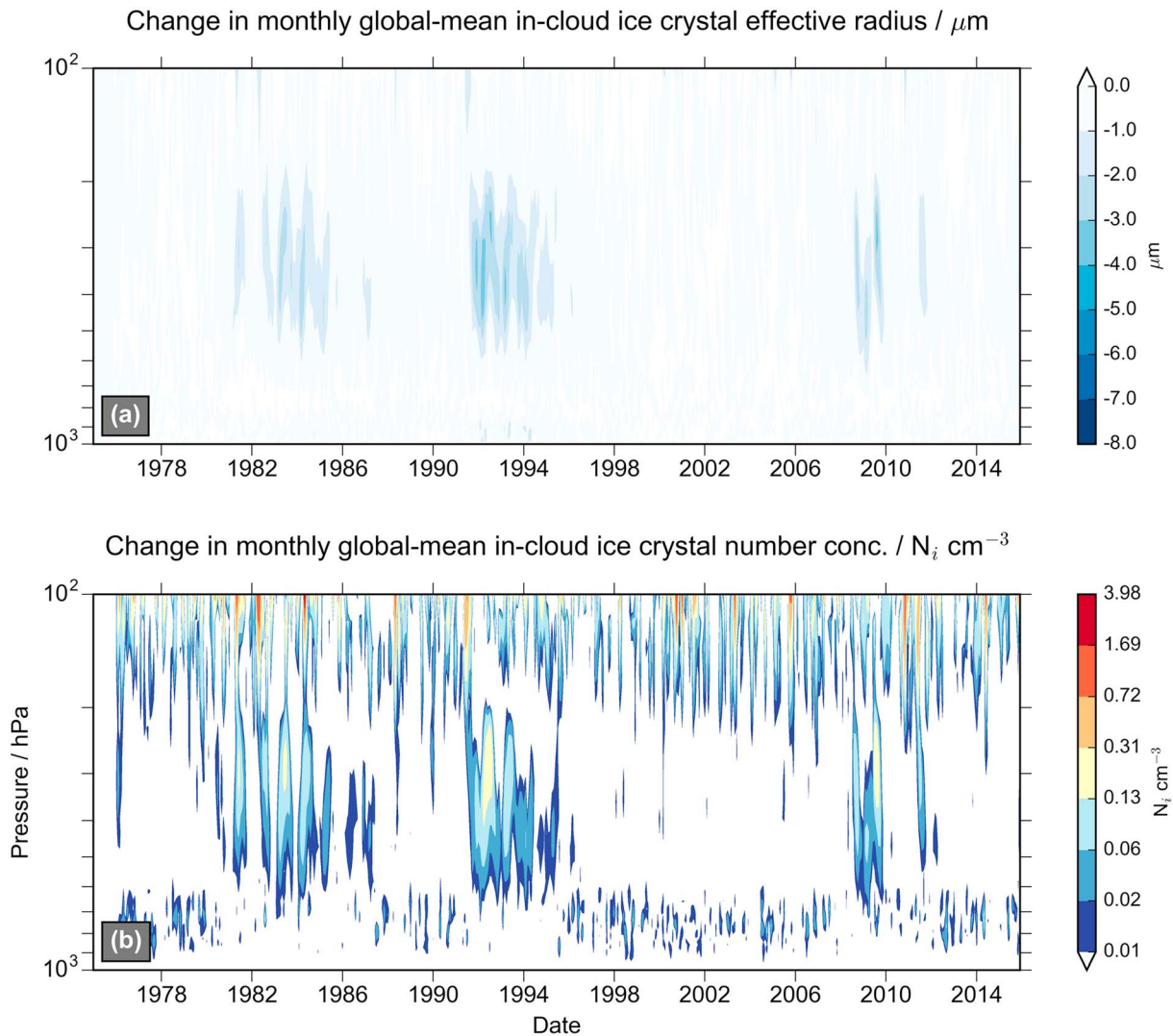


Figure 5. (a) Monthly global-mean changes in in-cloud ice crystal effective radius (μm) and (b) monthly global-mean changes in in-cloud ice crystal number concentrations (N_i/cm^3) diagnosed in CESM1-WACCM from simulations with and without volcanic sulfur dioxide emissions.

relation stems from the stratospheric adjusted forcing (i.e., only stratospheric temperatures are allowed to adjust) calculated by Hansen et al. (2005) in Goddard Institute for Space Studies (GISS) model E for the 1991 Mt. Pinatubo eruption. For 1991 Mt. Pinatubo simulations using prescribed sea surface temperature, which is equivalent to our model setup, ΔF equates to -26 W/m^2 per unit volcanic SAOD change (reported as SST-fixed forcing at <https://data.giss.nasa.gov/modelforce/strataer/>). We therefore use $\Delta F = -26 \text{ W/m}^2$ for the discussion and comparison of our results to IPCC AR5 from here onward.

Based on our nudged-*uv* prescribed sea surface temperature simulations, we calculate regression slopes of the annual global-mean total volcanic ERF against the annual global-mean volcanic SAOD change (Figure 6). We calculate a slope of $-21.5 \pm 1.1 \text{ W/m}^2$ for the combined periods 1982–1985 and 1990–1994 during which two large-magnitude eruptions took place. Importantly, the slope we calculate over these two time periods for large magnitude eruptions is $17 \pm 4\%$ less negative than reported in IPCC AR5 (Myhre et al., 2013). In our model this is mainly a result of the positive LW forcing from aerosol-cloud interactions (dLW_ERFaci) caused by an increase in the number concentration of ice crystals in the upper troposphere/lower stratosphere (Figure 5) as discussed in section 3.1. In addition, the sensitivity of ΔF to ΔSAOD depends on other factors such as the latitude and season of an eruption (Andersson et al., 2015;

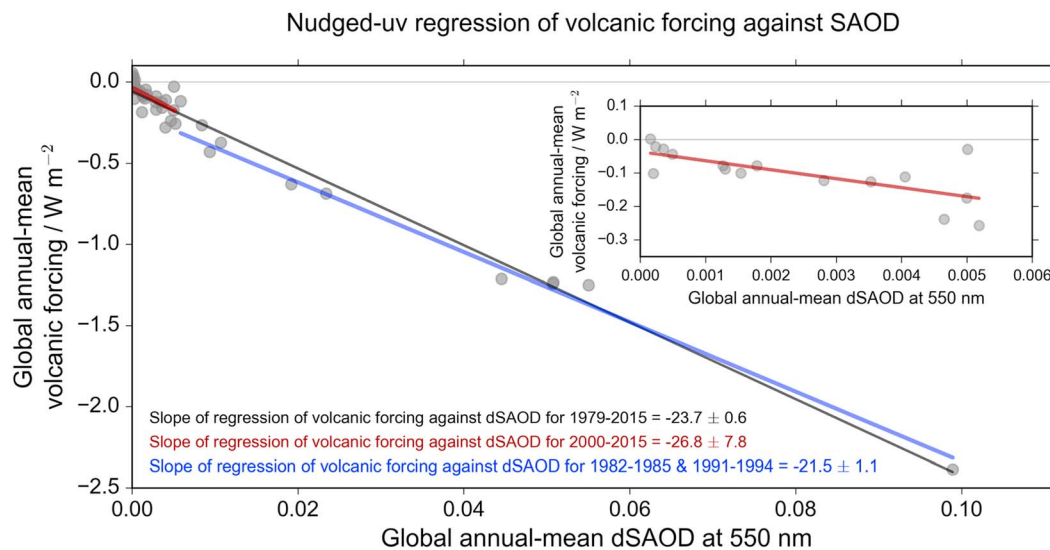


Figure 6. Regression of the annual global-mean total volcanic effective radiative forcing (W/m^2) against the annual global-mean stratospheric aerosol optical depth (SAOD at 550 nm) changes diagnosed in CESM1-WACCM for the periods 1979–2015 (black line), 1982–1985 and 1991–1994 combined (blue line), and 2000–2015 (dark red line). The inset figure shows the 2000–2015 period in detail.

Kravitz & Robock, 2011; Toohey et al., 2011) as well as differences in volcanic sulfate mass mixing ratio and aerosol particle sizes between eruptions of different magnitude. Large-magnitude eruptions such as 1982 El Chichón and 1991 Mt. Pinatubo result in greater sulfate mass mixing ratios (Figure S1) and increased aerosol particle size (Figure S2), disproportionately increasing the LW forcing relative to the SW forcing when compared to eruptions after 2004 (Figure 4). Sulfate aerosol particles with effective radii of about $0.25 \mu m$ scatter incoming solar radiation most efficiently per unit mass. The scattering efficiency per unit mass diminishes inversely with size for radii $>0.25 \mu m$ and is close to 0 for very small particles (Lacis, 2015; Lacis et al., 1992).

Previous studies also suggested that rapid adjustments act to reduce the total volcanic forcing to a similar or even larger degree compared to our study. For the 1991 Mt. Pinatubo eruption Hansen et al. (2005), who like us accounted for rapid adjustments in the troposphere as well as stratosphere, calculated a slope of $-23.0 W/m^2$ based on GISS model E simulations. Larson and Portmann (2016) calculated a multimodel mean slope of $-20.0 W/m^2$ for large-magnitude eruptions when analyzing CMIP5 simulations. Gregory et al. (2016) calculated slopes of $-17.0 \pm 1.0 W/m^2$ and $-19.0 \pm 0.5 W/m^2$ based on free-running atmosphere-ocean and atmosphere-only simulations with prescribed SAOD using the HadGEM2 model and the HadCM3 model. They found a positive ERFaci as a result of positive SW aerosol-cloud interaction effects, resulting from a reduction in cloud amount and/or cloud thickness following volcanic eruptions. In contrast, we find a negative SW forcing from aerosol-cloud interactions that for large-magnitude eruptions is outweighed by a positive LW forcing from aerosol-cloud interactions (Figure 4). Analyzing a set of free-running (i.e., without nudging but specifying time-varying historical sea surface temperatures and sea ice) CESM1(WACCM) simulations, we find a positive SW aerosol-cloud interactions effect, as in Gregory et al. (2016). This is not present in our nudged-uv simulations, likely as a result of neglecting dynamical impacts on clouds in this setup. Notwithstanding these differences in mechanisms between Gregory et al. (2016) and our study, all studies that accounted for rapid adjustments suggest a less negative total volcanic forcing compared to IPCC AR5 and CMIP5 for large-magnitude eruptions. The mechanisms by which rapid adjustments act to reduce the total volcanic forcing merit further investigation across different models and model setups. Based on our work, we suggest focusing on the magnitude and the sign of aerosol-cloud interactions diagnosed in different models and model setups.

For the period between 2000 and 2015, which was characterized by a series of small-to-moderate-magnitude eruptions, we obtain a slope of $-26.8 \pm 7.8 W/m^2$ in our nudged-uv model simulations in

Table 2
Observed Recurrence and Poisson Probabilities for (a) Volcanic Eruptions With Known Sulfur Dioxide Emissions Between 1980–2015 (a Period of $N = 36$ Years) With a Volcanic Explosivity Index (VEI; Newhall & Self, 1982), $VEI \geq 3$, and (b) for $VEI = 3, 4, \text{ and } 5$ Eruptions

(a) $VEI \geq 3$			
	$N = 36$	$dt = 1 \text{ yr}$	$\lambda = 1.83$
x	$p(x)$	$Np(x)$	Obs
0	0.160	5.756	5
1	0.293	10.552	11
2	0.269	9.673	11
3	0.164	5.911	4
4	0.075	2.709	4
5	0.028	0.993	1
6	0.008	0.304	0
7	0.002	0.079	0

(b) $VEI = 3, 4, 5$			
	$N = 36$	$dt = 1 \text{ yr}$	$\lambda = 1.81$
x	$p(x)$	$Np(x)$	Obs
0	0.164	5.918	5
1	0.297	10.685	12
2	0.268	9.646	10
3	0.161	5.806	4
4	0.073	2.621	4
5	0.026	0.946	1
6	0.008	0.285	0
7	0.002	0.073	0

Note. The volcanic sulfur dioxide emission inventory is compiled in Neely and Schmidt (2016). $p(x) = \lambda^x e^{-\lambda}/x!$; x = number of occurrences (or absence) of eruptions in given VEI category; λ = mean number of eruptions per dt ; $p(x)$ = Poisson probability; $Np(x)$ = calculated expected number of eruptions; Obs = number of eruptions based on database; N = number of years of data; dt = time interval of data.

close agreement with the stratospherically adjusted relation reported in IPCC AR5. In our model, however, the standard deviation on the calculated value of the slope is large and the magnitude of the net global mean radiative flux difference between the model and the satellite-derived fluxes for the years 2006 and 2011 is overestimated by up to -0.74 W/m^2 (2006–2001 mean of -0.15 W/m^2 ; Figure 3). Initiatives such as The Interactive Stratospheric Aerosol Model Inter-comparison Project (ISA-MIP; Timmreck et al., 2018) are directed at improving the accuracy of the calculations presented here.

Taken together, our work and that by Hansen et al. (2005), Gregory et al. (2016), and Larson and Portmann (2016) suggest that the IPCC AR5 volcanic forcings for large-magnitude eruptions ($VEI \geq 6$) are likely too negative. The notion of a reduced total volcanic forcing per unit SAOD change is in stark contrast to a previous study by Ge et al. (2016) suggesting that the IPCC AR5 formula of $\Delta F = -26 \text{ W/m}^2$ per unit volcanic SAOD (Myhre et al., 2013) is an underestimate by up to a factor of 3. The difference in results can be explained by the fact that Ge et al. (2016) do not account for the SW forcing from aerosol-cloud interactions and neglect all LW forcings in their calculation of the total volcanic forcing. Figure 4 shows that the total LW forcing offsets a large fraction of the total SW forcing for the post-2004 period in particular.

A reduced total volcanic forcing has implications for Earth's energy budget. Comparing the time-integrated total forcing reported in IPCC AR5 to ours (see Table 1 for annual-mean volcanic and total forcings), we find that for the Pinatubo period (1991–1996) about 17% more energy (or about $+59 \text{ MJ/m}^2$ over that time period) has accumulated in the Earth system, and about 3.6% more energy (or about $+24 \text{ MJ/m}^2$) between 1979 and 2011.

3.3. Frequency of Small-to-Moderate-Magnitude Eruptions and Implications for Stratospheric Aerosol Budget and Surface Temperature Changes

From Figure 2 it is apparent that small-to-moderate-magnitude volcanic eruptions with column heights $\geq 10 \text{ km}$ and SO_2 emissions of at least 0.01 Tg were less frequent between 1996 and 2002 than in the 1980s and the period 2005 to 2015. Although this is a relatively short time period, we used the SO_2 emission inventory (1979–2015) together with information on the VEI to understand how usual or unusual periods like the 1990s or the period 1996 to 2002 were. We find that occurrence and nonoccurrence of volcanic eruptions are statistically well described by a Poisson distribution, in line with previous studies (De la Cruz-Reyna, 1991; Roscoe, 2001), but extended here to $VEI = 3, 4, \text{ and } 5$ eruptions (Table 2). Importantly, we find that volcanically quiescent periods are rare: there is only a 16% chance of no $VEI \geq 3$ eruption occurring in any given year (i.e., a volcanically quiescent period) or inversely an 84% chance of at least one $VEI \geq 3$ eruption with column heights $\geq 10 \text{ km}$ and SO_2 emissions of at least 0.01 Tg occurring (i.e., a volcanically active period). The chance of the occurrence of one or two such eruptions in any given year is 57%, and the chance of three or more is 27% (Table 2). Therefore, the frequent occurrence of these small-to-moderate-magnitude eruptions ought to be accounted for in climate model simulations of past, present, and future climate change. The high frequency of these eruptions also has consequences for our understanding of the contribution of volcanic eruptions to the stratospheric aerosol budget and Earth's energy budget.

The majority of models that participated in CMIP5 did not account for volcanic aerosol forcing from small-to-moderate-magnitude eruptions after 2004 at all or prescribed global-mean SAOD values of 0.0001 from the year 2000 onward (Sato et al., 1993, and 2002 update; see also Schmidt et al., 2014), which was assumed to be representative of volcanically quiescent periods in the absence of large-magnitude eruptions. We apply the total volcanic ERF diagnosed in our model based on volcanic emissions in an energy budget model (that includes all natural and anthropogenic forcings; see section 2.3) to illustrate the effects of accounting for

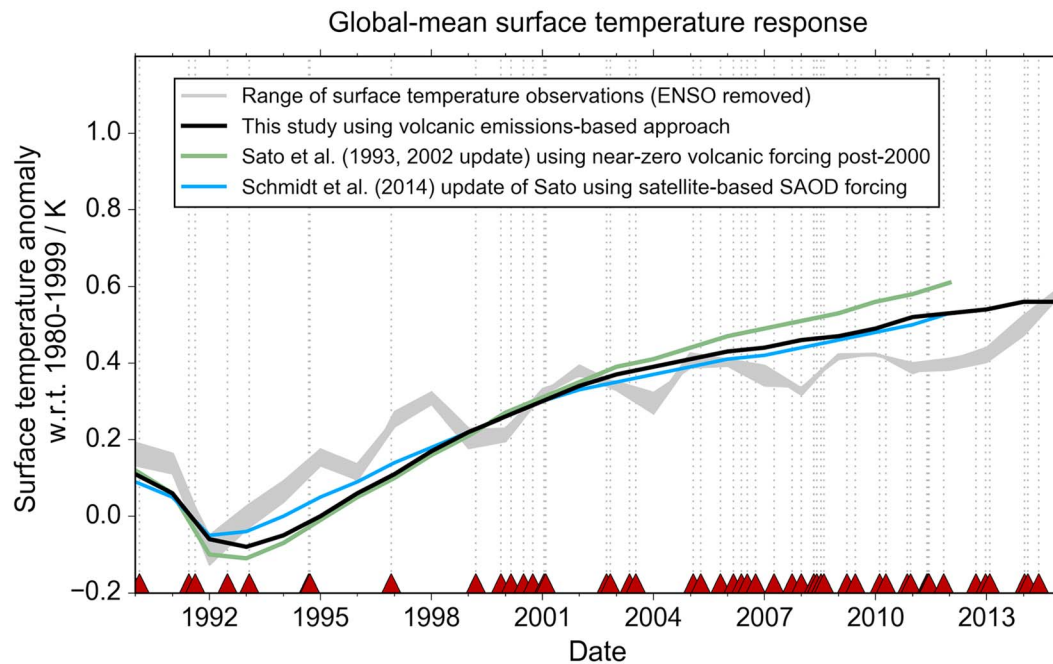


Figure 7. Global-mean surface temperature anomalies (with respect to 1980–1999 mean) calculated in an energy budget model (that includes all natural and anthropogenic forcings, see section 2.3) to illustrate the effects of volcanic eruptions post-1990 by applying the annual-mean volcanic ERF from the CESM1(WACCM) simulations (black line) and the volcanic forcings used by the majority of Coupled Model Inter-comparison Project version 5 (CMIP5) models (Sato et al., 1993, 2002 update; green line), and recent updates (Schmidt et al., 2014; blue line). All forcings applied in energy budget model are listed in Table 1. The difference between the green line and the black line illustrates that the effect of volcanic eruptions after 2004 is small (up to about -0.08 °C), but discernible in (model-simulated) global-mean decadal surface temperature changes. The grey shading shows the variability in surface temperature measurements based on three different data sets (Cowtan & Way, 2014; Hansen et al., 2010; Karl et al., 2015) for which ENSO variability has been removed.

frequent small-to-moderate-magnitude eruptions on surface temperature changes after 2004. We compare our results to surface temperature observations and to Schmidt et al. (2014) who repeated CMIP5 simulations using up-to-date satellite-based SAOD estimates. The grey shading in Figure 7 highlights the range of global surface temperature changes based on three different data sets (Cowtan & Way, 2014; Hansen et al., 2010; Karl et al., 2015) from which El Niño–Southern Oscillation (ENSO) variability has been removed (e.g., Huber & Knutti, 2014) using linear regression of each temperature data set against the December-January-February Oceanic Niño Index (NOAA, 2016b). Corroborating previous studies (Fyfe, von Salzen, et al., 2013; Ridley et al., 2014; Solomon et al., 2011), our energy budget model calculations illustrate that the effect of volcanic eruptions after 2004 is small (up to about -0.08 °C), but discernible in (model-simulated) global-mean decadal surface temperature changes (Figure 7, compare black and green lines). The effects of volcanic eruptions after 2004 are also detectable in lower tropospheric temperature measurements (Santer et al., 2014). The inclusion of the post-2004 volcanic ERF in our energy budget model reduces the gap between the observations and model-simulated temperature changes that apply a volcanic ERF representative of volcanic quiescence after the year 2000 (see green line in Figure 7) although the causes of this gap are manifold (e.g., Haywood et al., 2014; Marotzke & Forster, 2015; Monerie et al., 2017; Santer et al., 2014; Schmidt et al., 2014; Solomon et al., 2011). Further, the similarity of our model-simulated surface temperature changes and Schmidt et al. (2014) gives further confidence in our approach of using volcanic SO_2 emissions (compare black line in Figure 7 with the blue line based on satellite-derived SAOD values).

The upcoming CMIP6 experiments will be run prescribing volcanic SAOD reconstructions for the current and historical period up to the year 2014 (Eyring et al., 2016). After the year 2014, using a constant SAOD value of 0.01 has been proposed, which over the first 10 years will be ramped up linearly from zero to 0.01. The SAOD value of 0.01 is based on the average SAOD value calculated over the historical period that includes $\text{VEI} \geq 6$ eruptions (Eyring et al., 2016; O'Neill et al., 2016). The motivation behind using a constant SAOD value of 0.01

stems from the fact that neglecting volcanic forcing (in particular from $VEI \geq 6$ eruptions) will introduce long-term drift in ocean heat content, which in turn affects, for instance, predictions of sea level rise (Gregory, 2010; Gregory et al., 2013). However, $VEI \geq 6$ eruptions have a relatively low recurrence frequency of about 1 eruption every 50 to 60 years on average (Newhall & Self, 1982; Pyle, 1995). Therefore, prescribing a time-invariant historical mean SAOD of 0.01, which includes $VEI \geq 6$ events, may not always be the best approach, particularly if modeling groups wish to conduct model assessments of short-term (10 to 20 years) climate projections for periods during which $VEI \geq 6$ eruptions are assumed to be absent given their low recurrence frequency.

Next we quantify the average contribution of small-to-moderate-magnitude eruptions to the stratospheric aerosol budget, which enables modeling groups to account for these frequent eruptions in the absence of $VEI \geq 6$ eruptions. Based on the SO_2 emission inventory we calculate that an average mass of volcanic SO_2 of 0.48 Tg was emitted by all $VEI = 3, 4,$ or 5 eruptions with eruption column heights ≥ 15 km between 1979 and 2015. Using our model simulations we then calculate an annual mean ratio of volcanic SAOD to the mass of volcanic SO_2 emitted of 0.009 between the years 2000 and 2015 (when no $VEI \geq 6$ eruptions occurred). In the absence of large-magnitude eruptions, we find that small-to-moderate-magnitude eruptions increase the nonvolcanic background SAOD by about 0.004 on average (i.e., statistically representing one $VEI = 3, 4,$ or 5 eruption per year emitting 0.48 Tg of SO_2 , so $0.48 \text{ Tg} \times 0.009 \approx 0.004$). An SAOD enhancement of 0.004 equates to a volcanic ERF of -0.10 W/m^2 , which is about two thirds of the magnitude of the ERF from the ozone changes induced by ozone-depleting substances (Myhre et al., 2013). Compared to the nonvolcanic SAOD background of ~ 0.004 (based on 1998–2000 period in CMIP6 SAOD data set), these eruptions therefore contribute, on average, as much to the total SAOD as all nonvolcanic sources (including biomass burning, industrial combustion, mineral dust, meteoric smoke, and natural gaseous precursors such as carbonyl sulfide) combined during periods when large-magnitude eruptions are absent. A recent study by Friberg et al. (2018) using the Cloud-Aerosol Lidar with Orthogonal Polarization (CALIOP) instrument found a similar relative contribution of 40% on average to the total SAOD for the period 2006 to 2015.

4. Summary and Conclusions

We derived a time series of global-mean volcanic ERF, which accounts for rapid adjustments including aerosol perturbations of clouds, for the period 1979 to 2015 using a volcanic sulfur dioxide emission inventory in CESM1(WACCM). CESM1(WACCM) is a comprehensive climate model with interactive sulfur chemistry and a prognostic stratospheric aerosol scheme. From our emission-based model simulations we calculated a global multiannual mean volcanic ERF of -0.12 W/m^2 during 2005–2015 relative to a simulation without volcanic sulfur dioxide emissions. Relative to the volcanically quiescent 1999–2002 period, the volcanic ERF is -0.08 W/m^2 due to a series of small-to-moderate-magnitude explosive eruptions after 2004 (Table 1 and Figure 2), which is in good agreement with previous studies that used satellite-based volcanic aerosol forcings (Andersson et al., 2015; Ridley et al., 2014; Solomon et al., 2011). A volcanic ERF of -0.08 W/m^2 , albeit small, is significant as it offsets about one-third of the change in global-mean CO_2 forcing between the periods 1999–2002 and 2005–2015.

Using the method described by Ghan (2013), we decomposed the total volcanic ERF into contributions from aerosol-radiation interactions and aerosol-cloud interactions (Figures 2 and 4). In line with a small number of previous studies that diagnosed volcanic ERFs (Gregory et al., 2016; Hansen et al., 2005; Larson & Portmann, 2016), we found that rapid adjustments act to reduce the total volcanic ERF for large-magnitude explosive eruptions such as 1991 Mt. Pinatubo compared to the stratospherically adjusted forcing reported in IPCC AR5. The stratospherically adjusted forcing does not account for rapid adjustments such as cloud responses due to aerosol or radiative heating among other processes. Taken together, our work and that by Hansen et al. (2005), Gregory et al. (2016), and Larson and Portmann (2016) suggest that for large-magnitude eruptions such as 1982 El Chichón and 1991 Mt. Pinatubo, the relation between volcanic forcing and volcanic stratospheric optical depth (SAOD) is 13–21% weaker than reported in IPCC AR5. In our model, the reduced volcanic ERF is caused primarily by a large radiative effect in the LW from aerosol-cloud interactions that result from an increase in ice crystal number concentrations (yellow line in Figure 4 and Figure 5). However, the occurrence of any such changes in ice crystal number concentrations following volcanic

eruptions remains equivocal in observations and strongly dependent on freezing parameterizations in models, thus meriting further investigation. We suggest that multimodel initiatives such as ISA-MIP (Timmreck et al., 2018) focus on the analysis of the magnitude and the sign of aerosol-cloud interactions diagnosed in different models and model setups.

Overall, a reduced total volcanic forcing has implications not only for the relation between volcanic forcing and volcanic SAOD (Figure 6) but also Earth's energy budget and surface temperature changes (Figure 7) as reported in IPCC AR5, as well as the effectiveness of geoengineering using sulfate aerosol to mitigate climate change. Specifically, for the Pinatubo period (1991–1996) our simulations suggest that about 17% more energy than reported by IPCC AR5 has accumulated in the Earth system and about 3.6% more energy between 1979 and 2011.

To understand whether the apparent high occurrence frequency of eruptions during the period 2005–2015 was unusual or not, we carried out a statistical analysis of the recurrence frequency of small-to-moderate-magnitude eruptions ($VEI = 3, 4, \text{ or } 5$), column heights ≥ 10 km, and SO_2 emissions of at least 0.01 Tg between 1979 and 2015. We found that the occurrence and nonoccurrence of $VEI = 3, 4, \text{ or } 5$ eruptions are statistically well described by a Poisson distribution (Table 2) with a 57% chance of the occurrence of one or two eruptions of $VEI = 3, 4, \text{ or } 5$ in any given year. Notably, we argue that volcanically quiescent periods like the one between 1996 and 2002 are rare with only a small chance of 16% of no $VEI \geq 3$ eruption occurring in any given year. Taken together, our statistical analysis suggests that the volcanically active period between 2005 and 2015 was not unusual in terms of occurrence frequency of eruptions.

Given that volcanically quiescent periods and $VEI \geq 6$ eruptions are statistically rarer than periods of frequent small-to-moderate-magnitude eruptions ($VEI 3 \text{ or } 4 \text{ or } 5$), these more frequent eruptions should be accounted for in past, present, and future assessments of volcanic forcing of global climate change as well as in generating realistic near-term climate forcing scenarios assuming the absence of large-magnitude eruptions. In addition, such information on the probability of occurrence of eruptions and their stratospheric aerosol perturbations is also important for estimates of stratospheric ozone loss, which have been shown to be dependent on aerosol assumptions. For example, Solomon et al. (2016) showed that aerosols from small-to-moderate-magnitude eruptions influenced the recovery of the Antarctic ozone hole. From our model simulations we estimated that small-to-moderate-magnitude eruptions increase, on average, the nonvolcanic background SAOD by about 0.004 and thus contribute about 50% to the total SAOD in the absence of large-magnitude eruptions. This equates to a volcanic ERF of -0.10 W/m^2 , which is about two thirds of the magnitude of the ERF from the ozone changes induced by ozone-depleting substances (Myhre et al., 2013). Modeling groups who prescribe SAOD values and wish to run near-term climate projection simulations assuming an absence of large-magnitude eruptions could therefore use a global mean SAOD value of 0.004 on top of their nonvolcanic background value to account for frequent small-to-moderate-magnitude eruptions.

Paired with enhanced aerosol-chemistry-climate modeling capabilities, long-term remote ground-based and satellite-based measurements (e.g., Carn et al., 2016), there is ever increasing recognition and understanding of the high occurrence frequency and the role of small-to-moderate-magnitude eruptions in contributing to the stratospheric aerosol budget. Continued research efforts are needed to better understand and quantify the role of rapid adjustments including liquid water cloud and ice cloud responses in affecting the total volcanic forcing in particular for large-magnitude eruptions such as 1991 Mt. Pinatubo. To do so effectively, continued monitoring of volcanic activity and deriving accurate information on the mass of SO_2 emitted, volcanic plume heights as well as measurements of the microphysical and chemical evolution of volcanic plumes dispersion are vital to initiate and evaluate climate model simulations of volcanic eruptions.

References

- Allan, R. P., Liu, C., Loeb, N. G., Palmer, M. D., Roberts, M., Smith, D., & Vidale, P.-L. (2014). Changes in global net radiative imbalance 1985–2012. *Geophysical Research Letters*, *41*, 5588–5597. <https://doi.org/10.1002/2014GL060962>
- Andersson, S. M., Martinsson, B. G., Vernier, J.-P., Friberg, J., Brenninkmeijer, C. A. M., Hermann, M., van Velthoven, P. F. J., et al. (2015). Significant radiative impact of volcanic aerosol in the lowermost stratosphere. *Nature Communications*, *6*(1), 7692. <https://doi.org/10.1038/ncomms8692>
- Bingen, C., Robert, C. E., Stebel, K., Brühl, C., Schalllock, J., Vanhellefont, F., Mateshvili, N., et al. (2017). Stratospheric aerosol data records for the climate change initiative: Development, validation and application to chemistry-climate modelling. *Remote Sensing of Environment*, *203*, 296–321. <https://doi.org/10.1016/j.rse.2017.06.002>

Acknowledgments

First and foremost, A. S. would like to thank her baby daughter Lexi for sleeping well around the time when the revisions for this paper were due—what a star! A. S. received funding as visiting researcher from the National Center for Atmospheric Research (NCAR). P. M. F., A. S., R. A., and J. M. G. received funding from UK Natural Environment Research Council (NERC) grants NE/N006038/1 and NE/N006054/1 (SMURPHS). J. M. G. was also supported by the NCAS climate program. We would like to acknowledge high-performance computing support from Yellowstone (ark:/85065/d7wd3xhc) provided by NCAR's Computational and Information Systems Laboratory. NCAR is sponsored by the National Science Foundation. Any opinions, findings, and conclusions or recommendations expressed in the publication are those of the authors and do not necessarily reflect the views of the National Science Foundation. The Pacific Northwest National Laboratory (PNNL) is operated for the Department of Energy (DOE) by Battelle Memorial Institute under contract DE-AC06-76RLO 1830. Work at PNNL was supported by the U.S. DOE Earth System Modeling program. S. S. is partly supported by a grant from the National Science Foundation, 1539972. A. S. thanks Gavin Schmidt, Nicolas Bellouin, Thomas Aubry, and Amanda Maycock for very helpful discussions of this work. We also thank Valentina Aquila, Daniele Visioni, and an anonymous reviewer for their useful and constructive comments that helped to improve this paper. The output of all model simulations discussed in this study are available at the NCAR Earth System Grid at [doi:10.5065/D6C53JPS](https://doi.org/10.5065/D6C53JPS).

- Brühl, C., Lelieveld, J., Tost, H., Höpfner, M., & Glatthor, N. (2015). Stratospheric sulfur and its implications for radiative forcing simulated by the chemistry climate model EMAC. *Journal of Geophysical Research: Atmospheres*, *120*, 2103–2118. <https://doi.org/10.1002/2014JD022430>
- Carr, S. A., Clarisse, L., & Prata, A. J. (2016). Multi-decadal satellite measurements of global volcanic degassing. *Journal of Volcanology and Geothermal Research*, *311*, 99–134. <https://doi.org/10.1016/j.jvolgeores.2016.01.002>
- Cirisan, A., Spichtinger, P., Luo, B. P., Weisenstein, D. K., Wernli, H., Lohmann, U., & Peter, T. (2013). Microphysical and radiative changes in cirrus clouds by geoengineering the stratosphere. *Journal of Geophysical Research: Atmospheres*, *118*, 4533–4548. <https://doi.org/10.1002/jgrd.50388>
- Cowan, K., & Way, R. G. (2014). Coverage bias in the HadCRUT4 temperature series and its impact on recent temperature trends. *Quarterly Journal of the Royal Meteorological Society*, *140*(683), 1935–1944. <https://doi.org/10.1002/qj.2297>
- De la Cruz-Reyna, S. (1991). Poisson-distributed patterns of explosive eruptive activity. *Bulletin of Volcanology*, *54*(1), 57–67. <https://doi.org/10.1007/BF00278206>
- Diehl, T., Heil, A., Chin, M., Pan, X., Streets, D., Schultz, M., & Kinne, S. (2012). Anthropogenic, biomass burning, and volcanic emissions of black carbon, organic carbon, and SO₂ from 1980 to 2010 for hindcast model experiments. *Atmospheric Chemistry and Physics Discussions*, *12*(9), 24,895–24,954. <https://doi.org/10.5194/acpd-12-24895-2012>
- Eyring, V., Bony, S., Meeh, G. A., Senior, C. A., Stevens, B., Stouffer, R. J., & Taylor, K. E. (2016). Overview of the Coupled Model Intercomparison Project Phase 6 (CMIP6) experimental design and organization. *Geoscientific Model Development*, *9*(5), 1937–1958. <https://doi.org/10.5194/gmd-9-1937-2016>
- Forster, P. M., & Gregory, J. M. (2006). The climate sensitivity and its components diagnosed from Earth radiation budget data. *Journal of Climate*, *19*(1), 39–52. <https://doi.org/10.1175/JCLI3611.1>
- Forster, P. M., Richardson, T., Maycock, A. C., Smith, C. J., Samset, B. H., Myhre, G., Andrews, T., et al. (2016). Recommendations for diagnosing effective radiative forcing from climate models for CMIP6. *Journal of Geophysical Research: Atmospheres*, *121*, 12,460–12,475. <https://doi.org/10.1002/2016JD025320>
- Forster, P. M. F., & Taylor, K. E. (2006). Climate Forcings and climate sensitivities diagnosed from coupled climate model integrations. *Journal of Climate*, *19*(23), 6181–6194. <https://doi.org/10.1175/JCLI3974.1>
- Friberg, J., Martinsson, B. G., Andersson, S. M., & Sandvik, O. S. (2018). Volcanic impact on the climate—The stratospheric aerosol load in the period 2006–2015. *Atmospheric Chemistry and Physics Discussions*, *2018*, 1–35.
- Friberg, J., Martinsson, B. G., Sporre, M. K., Andersson, S. M., Brenninkmeijer, C. A. M., Hermann, M., van Velthoven, P. F. J., et al. (2015). Influence of volcanic eruptions on midlatitude upper tropospheric aerosol and consequences for cirrus clouds. *Earth and Space Science*, *2*, 285–300. <https://doi.org/10.1002/2015EA000110>
- Fromm, M., Kablick, G., Nedoluha, G., Carboni, E., Grainger, R., Campbell, J., & Lewis, J. (2014). Correcting the record of volcanic stratospheric aerosol impact: Nabro and Sarychev peak. *Journal of Geophysical Research: Atmospheres*, *119*, 10,343–310,364. <https://doi.org/10.1002/2014JD021507>
- Fyfe, J. C., Gillett, N. P., & Zwiers, F. W. (2013). Overestimated global warming over the past 20 years. *Nature Climate Change*, *3*(9), 767–769. <https://doi.org/10.1038/nclimate1972>
- Fyfe, J. C., von Salzen, K., Cole, J. N. S., Gillett, N. P., & Vernier, J. P. (2013). Surface response to stratospheric aerosol changes in a coupled atmosphere–ocean model. *Geophysical Research Letters*, *40*, 584–588. <https://doi.org/10.1002/grl.50156>
- Ge, C., Wang, J., Carn, S., Yang, K., Ginoux, P., & Krotkov, N. (2016). Satellite-based global volcanic SO₂ emissions and sulfate direct radiative forcing during 2005–2012. *Journal of Geophysical Research: Atmospheres*, *121*, 3446–3464. <https://doi.org/10.1002/2015JD023134>
- Gettelman, A., Liu, X., Barahona, D., Lohmann, U., & Chen, C. (2012). Climate impacts of ice nucleation. *Journal of Geophysical Research*, *117*, D20201. <https://doi.org/10.1029/2012JD017950>
- Gettelman, A., Liu, X., Ghan, S. J., Morrison, H., Park, S., Conley, A. J., Klein, S. A., et al. (2010). Global simulations of ice nucleation and ice supersaturation with an improved cloud scheme in the Community Atmosphere Model. *Journal of Geophysical Research*, *115*, D18216. <https://doi.org/10.1029/2009JD013797>
- Ghan, S. J. (2013). Technical note: Estimating aerosol effects on cloud radiative forcing. *Atmospheric Chemistry and Physics*, *13*(19), 9971–9974. <https://doi.org/10.5194/acp-13-9971-2013>
- Ghan, S. J., Liu, X., Easter, R. C., Zaveri, R., Rasch, P., Yoon, J.-H., & Eaton, B. (2012). Toward a minimal representation of aerosols in climate models: Comparative decomposition of aerosol direct, semidirect, and indirect radiative forcing. *Journal of Climate*, *25*(19), 6461–6476. <https://doi.org/10.1175/JCLI-D-11-00650.1>
- Gregory, J. M. (2010). Long-term effect of volcanic forcing on ocean heat content. *Geophysical Research Letters*, *37*, L22701. <https://doi.org/10.1029/2010GL045507>
- Gregory, J. M., Andrews, T., Good, P., Mauritsen, T., & Forster, P. M. (2016). Small global-mean cooling due to volcanic radiative forcing. *Climate Dynamics*, 1–13.
- Gregory, J. M., Bi, D., Collier, M. A., Dix, M. R., Hirst, A. C., Hu, A., Huber, M., et al. (2013). Climate models without preindustrial volcanic forcing underestimate historical ocean thermal expansion. *Geophysical Research Letters*, *40*, 1600–1604. <https://doi.org/10.1002/grl.50339>
- Hansen, J., Ruedy, R., Sato, M., & Lo, K. (2010). Global surface temperature change. *Reviews of Geophysics*, *48*, RG4004. <https://doi.org/10.1029/2010RG000345>
- Hansen, J., Sato, M., Ruedy, R., Nazarenko, L., Lacis, A., Schmidt, G. A., Russell, G., et al. (2005). Efficacy of climate forcings. *Journal of Geophysical Research*, *110*, D18104. <https://doi.org/10.1029/2005JD005776>
- Haywood, J. M., Jones, A., & Jones, G. S. (2014). The impact of volcanic eruptions in the period 2000–2013 on global mean temperature trends evaluated in the HadGEM2-ES climate model. *Atmospheric Science Letters*, *15*(2), 92–96. <https://doi.org/10.1002/asl2.471>
- Huber, M., & Knutti, R. (2014). Natural variability, radiative forcing and climate response in the recent hiatus reconciled. *Nature Geoscience*, *7*(9), 651–656. <https://doi.org/10.1038/ngeo2228>
- Hurrell, J. W., Hack, J. J., Shea, D., Caron, J. M., & Rosinski, J. (2008). A new Sea surface temperature and sea ice boundary dataset for the community atmosphere model. *Journal of Climate*, *21*(19), 5145–5153. <https://doi.org/10.1175/2008JCLI2292.1>
- IPCC (2013). In T. F. Stocker, D. Qin, G.-K. Plattner, M. Tignor, S. K. Allen, J. Boschung, et al. (Eds.), *Annex II: Climate system scenario tables in climate change 2013: The physical science basis. Contribution of Working Group I to the Fifth Assessment Report of the Intergovernmental Panel on Climate Change*, (pp. 1395–1446). Cambridge, United Kingdom and New York, NY, USA: Cambridge Univ. Press.
- Jensen, E. J., & Toon, O. B. (1992). The potential effects of volcanic aerosols on cirrus cloud microphysics. *Geophysical Research Letters*, *19*(17), 1759–1762. <https://doi.org/10.1029/92GL01936>
- Karl, T. R., Arguez, A., Huang, B., Lawrimore, J. H., McMahon, J. R., Menne, M. J., Peterson, T. C., et al. (2015). Possible artifacts of data biases in the recent global surface warming hiatus. *Science*, *348*(6242), 1469–1472. <https://doi.org/10.1126/science.aaa5632>

- Kooperman, G. J., Pritchard, M. S., Ghan, S. J., Wang, M., Somerville, R. C. J., & Russell, L. M. (2012). Constraining the influence of natural variability to improve estimates of global aerosol indirect effects in a nudged version of the Community Atmosphere Model 5. *Journal of Geophysical Research*, *117*, D23204. <https://doi.org/10.1029/2012JD018588>.
- Kravitz, B., & Robock, A. (2011). Climate effects of high-latitude volcanic eruptions: Role of the time of year. *Journal of Geophysical Research*, *116*, D01105. <https://doi.org/10.1029/2010JD014448>
- Kuebbeler, M., Lohmann, U., & Feichter, J. (2012). Effects of stratospheric sulfate aerosol geo-engineering on cirrus clouds. *Geophysical Research Letters*, *39*, L23803. <https://doi.org/10.1029/2012GL053797>
- Lacis, A. (2015). Volcanic aerosol radiative properties. *PAGES*, *23*(2), 50–51.
- Lacis, A., Hansen, J., & Sato, M. (1992). Climate forcing by stratospheric aerosols. *Geophysical Research Letters*, *19*(15), 1607–1610. <https://doi.org/10.1029/92GL01620>
- Larson, E. J. L., & Portmann, R. W. (2016). A temporal kernel method to compute effective radiative forcing in CMIP5 transient simulations. *Journal of Climate*, *29*(4), 1497–1509. <https://doi.org/10.1175/JCLI-D-15-0577.1>
- Loeb, N. G., Doelling, D. R., Wang, H., Su, W., Nguyen, C., Corbett, J. G., Liang, L., et al. (2017). Clouds and the Earth's radiant energy system (CERES) energy balanced and filled (EBAF) top-of-atmosphere (TOA) Edition-4.0 Data Product. *Journal of Climate*, *31*(2), 895–918.
- Loeb, N. G., Kato, S., Su, W., Wong, T., Rose, F. G., Doelling, D. R., Norris, J. R., et al. (2012). Advances in understanding top-of-atmosphere radiation variability from satellite observations. *Surveys in Geophysics*, *33*(3–4), 359–385. <https://doi.org/10.1007/s10712-012-9175-1>
- Lohmann, U., Kärcher, B., & Timmreck, C. (2003). Impact of the Mount Pinatubo eruption on cirrus clouds formed by homogeneous freezing in the ECHAM4 GCM. *Journal of Geophysical Research*, *108*, 4568. <https://doi.org/10.1029/2002JD003185>
- Luo, Z., Rossow, W. B., Inoue, T., & Stubenrauch, C. J. (2002). Did the eruption of the Mt. Pinatubo volcano affect cirrus properties? *Journal of Climate*, *15*(19), 2806–2820. [https://doi.org/10.1175/1520-0442\(2002\)015<2806:DTEOTM>2.0.CO;2](https://doi.org/10.1175/1520-0442(2002)015<2806:DTEOTM>2.0.CO;2)
- Marotzke, J., & Forster, P. M. (2015). Forcing, feedback and internal variability in global temperature trends. *Nature*, *517*(7536), 565–570. <https://doi.org/10.1038/nature14117>
- Meinshausen, M., Smith, S. J., Calvin, K., Daniel, J. S., Kainuma, M. L. T., Lamarque, J.-F., Matsumoto, K., et al. (2011). The RCP greenhouse gas concentrations and their extensions from 1765 to 2300. *Climatic Change*, *109*(1–2), 213–241. <https://doi.org/10.1007/s10584-011-0156-z>
- Mills, M. J., Richter, J. H., Tilmes, S., Kravitz, B., MacMartin, D. G., Glanville, A. A., Tribbia, J. J., et al. (2017). Radiative and chemical response to interactive stratospheric sulfate aerosols in fully coupled CESM1(WACCM). *Journal of Geophysical Research: Atmospheres*, *122*, 13,061–13,078. <https://doi.org/10.1002/2017JD027006>
- Mills, M. J., Schmidt, A., Easter, R., Solomon, S., Kinnison, D. E., Ghan, S. J., Neely, R. R., et al. (2016). Global volcanic aerosol properties derived from emissions, 1990–2014, using CESM1(WACCM). *Journal of Geophysical Research: Atmospheres*, *121*, 2332–2348. <https://doi.org/10.1002/2015JD024290>
- Minnis, P., Harrison, E. F., Stowe, L. L., Gibson, G. G., Denn, F. M., Doelling, D. R., & Smith, W. L. (1993). Radiative climate forcing by the Mount Pinatubo eruption. *Science*, *259*(5100), 1411–1415. <https://doi.org/10.1126/science.2595100.1411>
- Monerie, P.-A., Moine, M.-P., Terray, L., & Valcke, S. (2017). Quantifying the impact of early 21st century volcanic eruptions on global-mean surface temperature. *Environmental Research Letters*, *12*(5), 054010. <https://doi.org/10.1088/1748-9326/aa6cb5>
- Morice, C. P., Kennedy, J. J., Rayner, N. A., & Jones, P. D. (2012). Quantifying uncertainties in global and regional temperature change using an ensemble of observational estimates: The HadCRUT4 data set. *Journal of Geophysical Research*, *117*, D08101. <https://doi.org/10.1029/2011JD017187>
- Morrison, H., & Gettelman, A. (2008). A new two-moment bulk Stratiform cloud microphysics scheme in the community atmosphere model, version 3 (CAM3). Part I: Description and numerical tests. *Journal of Climate*, *21*(15), 3642–3659. <https://doi.org/10.1175/2008JCLI2105.1>
- Myhre, G., Shindell, D., Bréon, F.-M., Collins, W., Fuglestvedt, J., Huang, J., Koch, D., et al. (2013). Anthropogenic and natural radiative forcing. In T. F. Stocker, D. Qin, G.-K. Plattner, M. Tignor, S. K. Allen, J. Boschung, et al. (Eds.), *Climate change 2013: The physical science basis. Contribution of Working Group I to the Fifth Assessment Report of the Intergovernmental Panel on Climate Change*, (pp. 659–740). Cambridge, United Kingdom and New York, NY, USA: Cambridge Univ. Press.
- Neely, R. R., and Schmidt, A. (2016). VolcanEESM: Global volcanic sulphur dioxide (SO₂) emissions database from 1850 to present - Version 1.0., Centre for Environmental Data Analysis.
- Newhall, C. G., & Self, S. (1982). The Volcanic Explosivity Index (VEI) an estimate of explosive magnitude for historical volcanism. *Journal of Geophysical Research*, *87*(C2), 1231–1238. <https://doi.org/10.1029/JC087iC02p01231>
- NOAA (2016a). AGGI, Edited.
- NOAA (2016b). ONI, Edited.
- O'Neill, B. C., Tebaldi, C., van Vuuren, D. P., Eyring, V., Friedlingstein, P., Hurtt, G., Knutti, R., et al. (2016). The Scenario Model Intercomparison Project (ScenarioMIP) for CMIP6. *Geoscientific Model Development*, *9*(9), 3461–3482. <https://doi.org/10.5194/gmd-9-3461-2016>
- Pyle, D. M. (1995). Mass and energy budgets of explosive volcanic eruptions. *Geophysical Research Letters*, *22*(5), 563–566. <https://doi.org/10.1029/95GL00052>
- Ridley, D. A., Solomon, S., Barnes, J. E., Burlakov, V. D., Deshler, T., Dolgii, S. I., Herber, A. B., et al. (2014). Total volcanic stratospheric aerosol optical depths and implications for global climate change. *Geophysical Research Letters*, *41*, 7763–7769. <https://doi.org/10.1002/2014GL061541>
- Rienecker, M. M., Suarez, M. J., Gelaro, R., Todling, R., Bacmeister, J., Liu, E., Bosilovich, M. G., et al. (2011). MERRA: NASA's Modern-Era Retrospective Analysis for Research and Applications. *Journal of Climate*, *24*(14), 3624–3648. <https://doi.org/10.1175/JCLI-D-11-00015.1>
- Roscoe, H. K. (2001). The risk of large volcanic eruptions and the impact of this risk on future ozone depletion. *Natural Hazards*, *23*(2/3), 231–246. <https://doi.org/10.1023/A:1011178016473>
- Santer, B. D., Bonfils, C., Painter, J. F., Zelinka, M. D., Mears, C., Solomon, S., Schmidt, G. A., et al. (2014). Volcanic contribution to decadal changes in tropospheric temperature. *Nature Geoscience*, *7*(3), 185–189. <https://doi.org/10.1038/ngeo2098>
- Sassen, K. (1992). Evidence for liquid-phase cirrus cloud formation from volcanic aerosols: Climatic implications. *Science*, *257*(5069), 516–519. <https://doi.org/10.1126/science.257.5069.516>
- Sato, M., Hansen, J. E., McCormick, M. P., & Pollack, J. B. (1993). Stratospheric aerosol optical depths, 1850–1990. *Journal of Geophysical Research*, *98*(D12), 22,987–22,994. <https://doi.org/10.1029/93JD02553>
- Schmidt, G. A., Shindell, D. T., & Tsigaridis, K. (2014). Reconciling warming trends. *Nature Geoscience*, *7*(3), 158–160. <https://doi.org/10.1038/ngeo2105>
- Solomon, S., Daniel, J. S., Neely, R. R., Vernier, J.-P., Dutton, E. G., & Thomason, L. W. (2011). The persistently variable “background” stratospheric aerosol layer and global climate change. *Science*, *333*(6044), 866–870. <https://doi.org/10.1126/science.1206027>
- Solomon, S., Ivy, D. J., Kinnison, D., Mills, M. J., Neely, R. R., & Schmidt, A. (2016). Emergence of healing in the Antarctic ozone layer. *Science*, *353*(6296), 269–274. <https://doi.org/10.1126/science.aae0061>

- Thomason, L. W., Ernest, N., Millán, L., Rieger, L., Bourassa, A., Vernier, J. P., Manney, G., et al. (2018). A global space-based stratospheric aerosol climatology: 1979–2016. *Earth System Science Data*, *10*(1), 469–492. <https://doi.org/10.5194/essd-10-469-2018>
- Timmreck, C., Mann, G. W., Aquila, V., Hommel, R., Lee, L. A., Schmidt, A., Brühl, C., et al. (2018). The Interactive Stratospheric Aerosol Model Intercomparison Project (ISA-MIP): Motivation and experimental design. *Geoscientific Model Development*, *11*(7), 2581–2608. <https://doi.org/10.5194/gmd-11-2581-2018>
- Toohey, M., Krüger, K., Niemeier, U., & Timmreck, C. (2011). The influence of eruption season on the global aerosol evolution and radiative impact of tropical volcanic eruptions. *Atmospheric Chemistry and Physics*, *11*(23), 12351–12367. <https://doi.org/10.5194/acp-11-12351-2011>
- Trenberth, K. E., & Fasullo, J. T. (2013). An apparent hiatus in global warming? *Earth's Future*, *1*(1), 19–32. <https://doi.org/10.1002/2013EF000165>
- Vernier, J. P., Thomason, L. W., Pommereau, J. P., Bourassa, A., Pelon, J., Garnier, A., Hauchecorne, A., et al. (2011). Major influence of tropical volcanic eruptions on the stratospheric aerosol layer during the last decade. *Geophysical Research Letters*, *38*, L12807. <https://doi.org/10.1029/2011GL047563>
- Visioni, D., Pitari, G., & di Genova, G. (2018). Upper tropospheric ice sensitivity to sulfate geoengineering. *Atmospheric Chemistry and Physics Discussions*, 1–37.
- Zhang, K., Wan, H., Liu, X., Ghan, S. J., Kooperman, G. J., Ma, P. L., Rasch, P. J., et al. (2014). Technical note: On the use of nudging for aerosol–climate model intercomparison studies. *Atmospheric Chemistry and Physics*, *14*(16), 8631–8645. <https://doi.org/10.5194/acp-14-8631-2014>